THE AMERICAN SOCIETY OF MECHANICAL ENGINEERS
345 E. 47th St., New York, N.Y. 10017

98-GT-265

Rotating Stall Control in a High-Speed Stage with Inlet Distortion, Part II – Circumferential Distortion

Z. S. Spakovszky
Gas Turbine Laboratory
Department of Aeronautics and Astronautics
Massachusetts Institute of Technology
Cambridge, MA 02139

C. M. van Schalkwyk
Scientific Systems Co., Inc.
Woburn, MA 01801

H. J. Weigl, J. D. Paduano
Gas Turbine Laboratory
Department of Aeronautics and Astronautics
Massachusetts Institute of Technology
Cambridge, MA 02139

K. L. Suder, M. M. Bright
NASA Lewis Research Center
Cleveland, OH 44135

Abstract

This paper presents the first attempt to stabilize rotating stall in a single-stage transonic axial flow compressor with inlet distortion using active feedback control. The experiments were conducted at the NASA Lewis Research Center on a single-stage transonic core compressor inlet stage. An array of 12 jet injectors located upstream of the compressor was used for forced response testing and feedback stabilization. Results for a circumferential total pressure distortion of about one dynamic head and a 120° extent (DC(60)=0.61) are reported in this paper. Part I (Spakovszky et al. (1998)) reports results for radial distortion.

Control laws were designed using empirical transfer function estimates determined from forced response results. Distortion introduces coupling between the harmonics of circumferential pressure perturbations, requiring multivariable identification and control design techniques. The compressor response displayed a strong first spatial harmonic, dominated by the well known incompressible Moore-Greitzer mode.

Steady axisymmetric injection of 4% of the compressor mass flow resulted in a 6.2% reduction of stalling mass flow. Constant gain feedback, using unsteady asymmetric injection, yielded a further range extension of 9%. A more sophisticated robust H_∞ controller allowed a reduction in stalling mass flow of 10.2% relative to steady injection, yielding a total reduction in stalling mass flow of 16.4%.

1. Introduction

For a better understanding of the coupled compressor dynamics a short overview of *undistorted* flow compressor modeling is given. The classic Moore-Greitzer formulation (Moore and Greitzer (1986)) considers an incompressible two-dimensional flow field with an axisymmetric, spatially uniform (undistorted) inlet flow, and a linearized approach for the perturbations. The rotating stall dynamics for the nth mode are described by

$$\left(\frac{2}{|n|}+\mu\right)\frac{\partial\delta\phi}{\partial\tau}=\left(\frac{\partial\Psi^{ts}}{\partial\phi}-jn\lambda\right)\delta\phi, \qquad (1)$$

where Ψ^{ts} is the total-to-static pressure rise coefficient of the entire compressor and ϕ and $\delta\phi$ are the compressor face flow coefficient and its perturbation respectively. The inertia parameters are the fluidic inertia in the rotors λ, in the rotors plus stators μ, and in the inlet and exit ducts $\frac{2}{|n|}$, where

$$\lambda=\sum_{\text{rotors}}\frac{c_x/\bar{r}}{\cos^2\xi}, \qquad \mu=\lambda+\sum_{\text{stators}}\frac{c_x/\bar{r}}{\cos^2\xi}. \qquad (2)$$

Presented at the International Gas Turbine & Aeroengine Congress & Exhibition
Stockholm, Sweden — June 2–June 5, 1998
This paper has been accepted for publication in the Transactions of the ASME
Discussion of it will be accepted at ASME Headquarters until September 30, 1998

c_x, $\bar{r}$, and ξ are the axial chord, mean radius, and stagger angle respectively. Solving Equation (1) with

$$\delta\phi(\theta,t) = \sum_{n=-\infty}^{\infty} \delta\tilde{\phi}_n(t)e^{jn\theta} \tag{3}$$

yields

$$\delta\phi(\theta,t) = \sum_{n=-\infty}^{\infty} a_n e^{(\sigma_n - jn\omega_n)t} e^{jn\theta}, \tag{4}$$

where θ and t are the angle around the annulus and the time respectively. The growth rate σ_n and rotation rate ω_n are given by

$$\sigma_n = \frac{\frac{\partial \Psi^{ts}}{\partial \phi}}{\left(\frac{2}{|n|} + \mu\right)}, \qquad \omega_n = \frac{\lambda}{\left(\frac{2}{|n|} + \mu\right)}. \tag{5}$$

This solution describes spatial waves of sinusoidal shape (harmonics) that travel around the annulus at rotation rate ω_n, and grow or decay in time with growth rate σ_n. Compressor stability is determined by the growth rate of these modes. In this model, the axial velocity perturbations $\delta\phi(\theta)$ are axially uniform throughout the compressor. Furthermore, the flow field for the nth mode consists only of the nth spatial harmonic. That is, the harmonics are all *decoupled* (independent of one another).

In the presence of circumferentially nonuniform inlet flow the pressure rise Ψ^{ts}, and therefore the slope $\frac{\partial \Psi^{ts}}{\partial \phi}$, is no longer a constant but a strong function of θ. This nonlinear coupling between the steady inlet flow field and the compressor map strongly influences the linearized behavior of the flow field perturbations. The mode shapes are no longer purely sinusoidal but have contributions of other harmonics. In other words, distortion introduces *coupling* between the harmonics. Hynes and Greitzer (1987) have extended the Moore-Greitzer model to describe incompressible dynamics with inlet distortion. The accuracy of this model has been verified experimentally by Van Schalkwyk et al. (1997) on a low-speed three-stage compressor.

If an analysis accounting for compressibility is done, acoustic modes with axial structure are introduced. In this case, each compression system mode has both circumferential and axial structure. Modeling of this kind was conducted by Bonnaure (1991), Hendricks et al. (1993), and Feulner et al. (1994). To date, no control-theoretic compressible model exists which accounts for inlet distortion. Thus it is one of the goals of this paper to investigate the effects of inlet distortion on high-speed compressor pre-stall behavior.

The other goals of this paper are identification and stabilization of the compression system with inlet distortion. Our framework will be, as in Part I (Spakovszky et al. (1998)), a multi-variable input-output characterization where measurements and actuation are expressed as complex spatial Fourier coefficients (Paduano et al. (1993)). This framework is consistent with the stability analysis of Hynes and Greitzer (1987), except their analysis was homogeneous instead of forced, and a nonlinear steady-state condition was found numerically (ours is achieved experimentally). The frequency domain input-output map, or transfer function matrix, for the first three harmonics is written:

$$\begin{bmatrix} \tilde{y}_0(s) \\ \tilde{y}_1(s) \\ \tilde{y}_2(s) \end{bmatrix} = \begin{bmatrix} G_{00}(s) & G_{01}(s) & G_{02}(s) \\ G_{10}(s) & G_{11}(s) & G_{12}(s) \\ G_{20}(s) & G_{21}(s) & G_{22}(s) \end{bmatrix} \begin{bmatrix} \tilde{u}_0(s) \\ \tilde{u}_1(s) \\ \tilde{u}_2(s) \end{bmatrix}, \tag{6}$$

or, in compact form,

$$\tilde{\mathbf{y}}(s) = \mathbf{G}(s)\tilde{\mathbf{u}}(s), \tag{7}$$

where the output vector $\tilde{\mathbf{y}}$ is a vector containing the system's primary outputs: the complex spatial Fourier coefficients (SFCs) of the pressure perturbations (analogous to Equation (3)). The input vector $\tilde{\mathbf{u}}$ contains the corresponding SFCs of the injection profile, which is the system input.

Coupling between harmonics due to circumferential distortion is indicated by nonzero off-diagonal elements of $\mathbf{G}(s)$ ($G_{ij}(s) \neq 0$ for all $i \neq j$). The strength of this coupling can be determined by the magnitudes of the off-diagonal transfer functions. The consequence of this coupling is that the individual transfer functions of $\mathbf{G}$ cannot be treated independently; thus controller design becomes a multi-input-multi-output (MIMO) problem. This increases the complexity of the controller and complicates system identification. After describing the steady-state conditions, we will use these concepts to interpret the identification and control results.

2. Experimental Setup

The experiments described in this paper were all conducted at the NASA Lewis Research Center in the single-stage axial compressor test facility. A detailed description of the NASA Stage 35 test compressor and the actuation and instrumentation is given in Part I (Spakovszky et al. (1998)), as well as other documents, Reid and Moore (1978), Berndt et al. (1995), Weigl et al. (1997), and will not be repeated here. For our purposes it suffices to say that a set of twelve evenly spaced injectors, blowing high pressure air in the tip region of the rotor, provide the actuation, and a set of 8

static pressure transducers located immediately upstream of the rotor provide sensing. Both the actuation and sensing signals are decomposed into spatial Fourier coefficients, and treated as such in the remainder of the paper.

3. Circumferential Inlet Distortion

An early effort using steady blowing and bleeding devices to determine if tip boundary layer control was an effective means of increasing the unstalled weight flow range of a transonic single-stage compressor with and without inlet flow distortion was conducted by Koch (1970). The experiments revealed that the blowing device was more effective than the bleed device and that the unstalled range could be improved. Circumferential inlet airflow distortion that is caused by phenomena such as flow separation or non-axisymmetric intake duct geometry has been studied by installing a circumferential distortion screen: a fine mesh was mounted in the inlet duct, located approximately 2.2 mean radii upstream of the rotor (as in Part I). The screen can be indexed through 350° around the annulus to allow more detailed mapping of steady state compressor performance. The extent of the screen was 120° and covered the full blade span.

3.1 Steady State Experiments

Circumferential total and static pressure and total temperature profiles were measured with probes positioned between the distortion screen and the rotor. In addition, four circumferentially distributed wall static pressure taps at the hub and casing, and a total pressure and total temperature rake provided data on the flow field downstream of the compressor. The steady pressure and temperature probes were geometrically fixed and the screen was rotated in five degree increments to obtain the profiles. Figure 1 shows the total and static pressure profiles at the inlet, approximately 1.1 mean radii upstream of the rotor inlet, and the static pressure profile at the compressor exit. The mean exit static pressure has been subtracted from all these curves to show the relative offset of the pressure profiles. The distortion screen blocked the flow between 120° and 240° circumferentially; these angles are marked with the dotted vertical lines in the figure. The total pressure drop generated by the distortion screen was about one dynamic head, that is

$$\frac{\Delta p_t}{\frac{1}{2}\bar{\rho}\bar{v}_x^2} \approx 1. \tag{8}$$

The distortion magnitude can also be described by a parameter commonly used in engine intake aerodynamics called

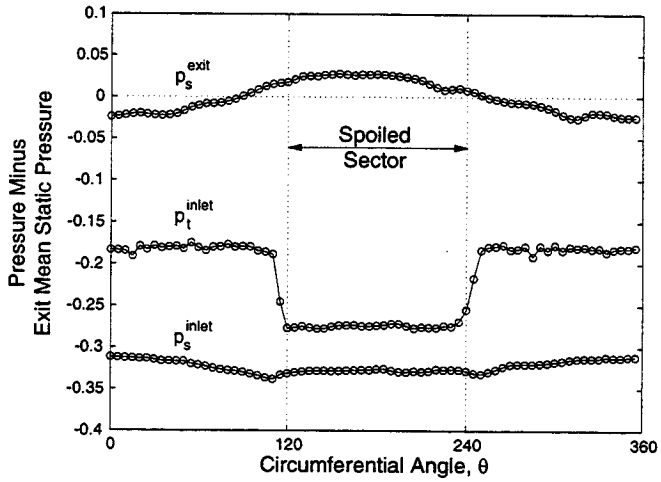

Figure 1: Total and static pressure at the compressor inlet and static pressure at the compressor exit for 1 dynamic head distortion at $\dot{m}_{corr} = 16.5$ kg/s without blowing.

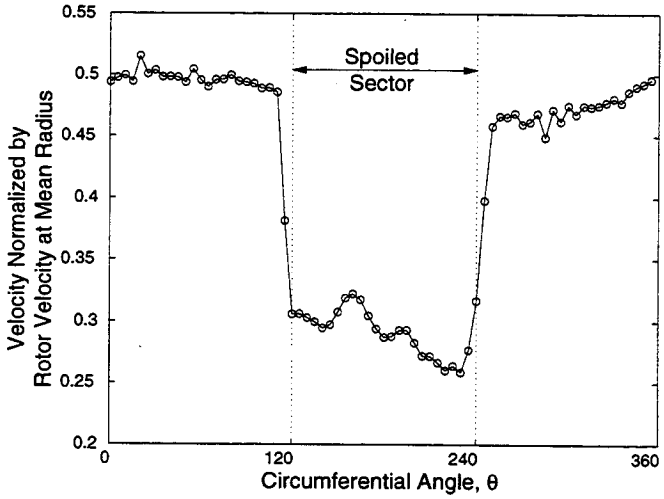

Figure 2: Measured velocity profile for 1 dynamic head distortion at $\dot{m}_{corr} = 16.5$ kg/s without blowing.

the DC(60) descriptor (Williams (1991)). The DC(60) descriptor is defined by

$$\mathrm{DC}(60) = \frac{\bar{p}_t|_{360°} - \bar{p}_t|_{\text{worst } 60°}}{\frac{1}{2}\rho\bar{v}_x^2}. \tag{9}$$

In the ideal case where the static pressure is uniform, DC(60)=1 corresponds to zero-velocity flow within the 60° sector, giving very poor inlet aerodynamics. The distortion screen designed for Stage 35 with 1 dynamic head distortion magnitude corresponds to DC(60)=0.61, representing poor inlet conditions, as shown in the velocity profile in Figure 2.

The inlet static pressure shown in Figure 1 is approximately uniform around the annulus, while the exit static pressure is circumferentially nonuniform with an increased pressure rise in the range $120° \leq \theta \leq 240°$. This contradicts the basic Hynes-Greitzer theory (Hynes and Greitzer (1987)) which assumes that the flow angle from the stator vanes is uniform and that the downstream duct has constant area. In a two-dimensional (incompressible) flow field these assumptions imply uniform exit static pressure and nonuniform inlet static pressure. This discrepancy between the theory and measurements can be explained by considering the compressor *plus* downstream diffuser, and using a parallel compressor type argument as follows (see Longley and Greitzer (1992)): In the spoiled sector the diffuser is operating with low inlet total pressure and thus low velocity, producing a lower pressure rise than the diffuser in the unspoiled sector. Since the static pressure at the diffuser exit must be uniform, the static pressure at the compressor exit must be higher in the spoiled sector than in the unspoiled sector.

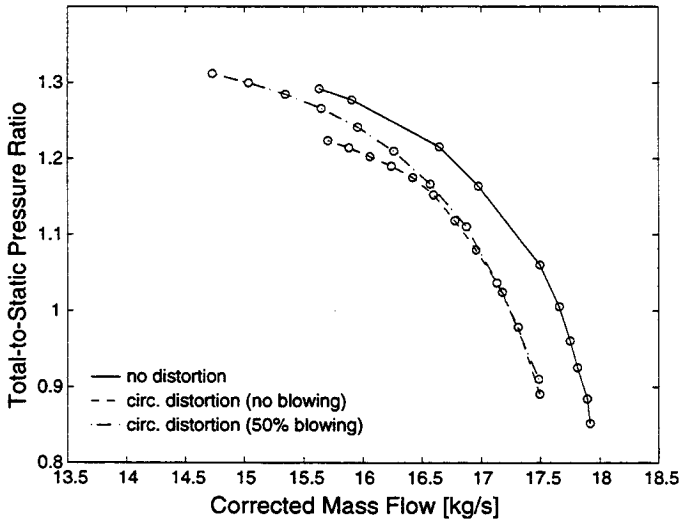

Figure 3: Speed lines for undistorted inlet (solid), circumferential distortion no blowing (dash), and with 50% steady blowing (dash-dot).

Speed lines were measured for undistorted inlet flow as well as with circumferential inlet distortion. The effect of steady blowing (steady valve opening of 50%, injected corrected mass flow of 0.65 kg/sec) on the pressure ratio was then measured. The speed lines are constructed as described in Part I: total corrected mass flow is the sum of an upstream orifice mass flow and the injected mass flow, the upstream total pressure is the mass average of total pressure probes between the distortion screen and the actuators, and the downstream pressure is from mass averaged hub and casing static pressure measurements. In Figure 3 we see that the circumferential distortion resulted in a peak pressure ratio drop. However, with steady blowing the peak pressure ratio can be recovered and even a considerable range extension of 6.2% in stalling mass flow can be obtained. Although the pressure ratio of the compressor is recovered by blowing, there is no change in the inlet distortion, because the distortion screen is upstream of the compressor, and there is considerable non-uniformity in the compressor face flow field, as evidenced by the system identification results in the next section.

4. Open Loop Compressor Dynamics

Having characterized the steady-state behavior, we turn to the dynamic behavior near stall. Using sinusoidal frequency sweeps on each spatial harmonic, we quantify the dominant eigenmodes of the system, their circumferential structure, and the degree of coupling between harmonics that exists in the input-output dynamics. The latter is important for control law design; it is also of interest to determine the degree of coupling between harmonics in *compressible* pre-stall modes.

Using standard frequency sweep methods (see Ljung (1987)), we measured the transfer function matrix (Equation (6)). The off-diagonal elements, $G_{ij}(j\omega)$ for $i \neq j$, were found to have magnitudes of about 0.1 to 1.0 times the diagonal elements, indicating strong coupling between some harmonics. A subset of the transfer functions is shown in Figure 4. The magnitudes of the off-diagonal transfer functions $G_{01}(j\omega)$ and $G_{10}(j\omega)$ are of the same order as the diagonal transfer functions $G_{00}(j\omega)$ and $G_{11}(j\omega)$. To find the eigenvalues, and for control law design, state-space models were identified based on the measured transfer functions using an MIT-developed method called FORSE (Jacques (1994)). The transfer functions of the identified state space model are plotted as dashed lines in Figure 4.

The peaks in the transfer functions indicate that there are several lightly damped modes in the pressure perturbations. Due to compressibility, several modes with similar circumferential structure can exist, each having different axial structure. Therefore we denote the modes by $[n, m]$, where n is inferred from the circumferential harmonic that is largest in the mode, and m indicates the postulated axial mode number (higher values of m indicate higher frequency, usually associated with more axial mode structure, as in acoustics)[1].

[1]The mode names used here are primarily for conveying the physical effects involved, and do not effect controller design at all; controllers

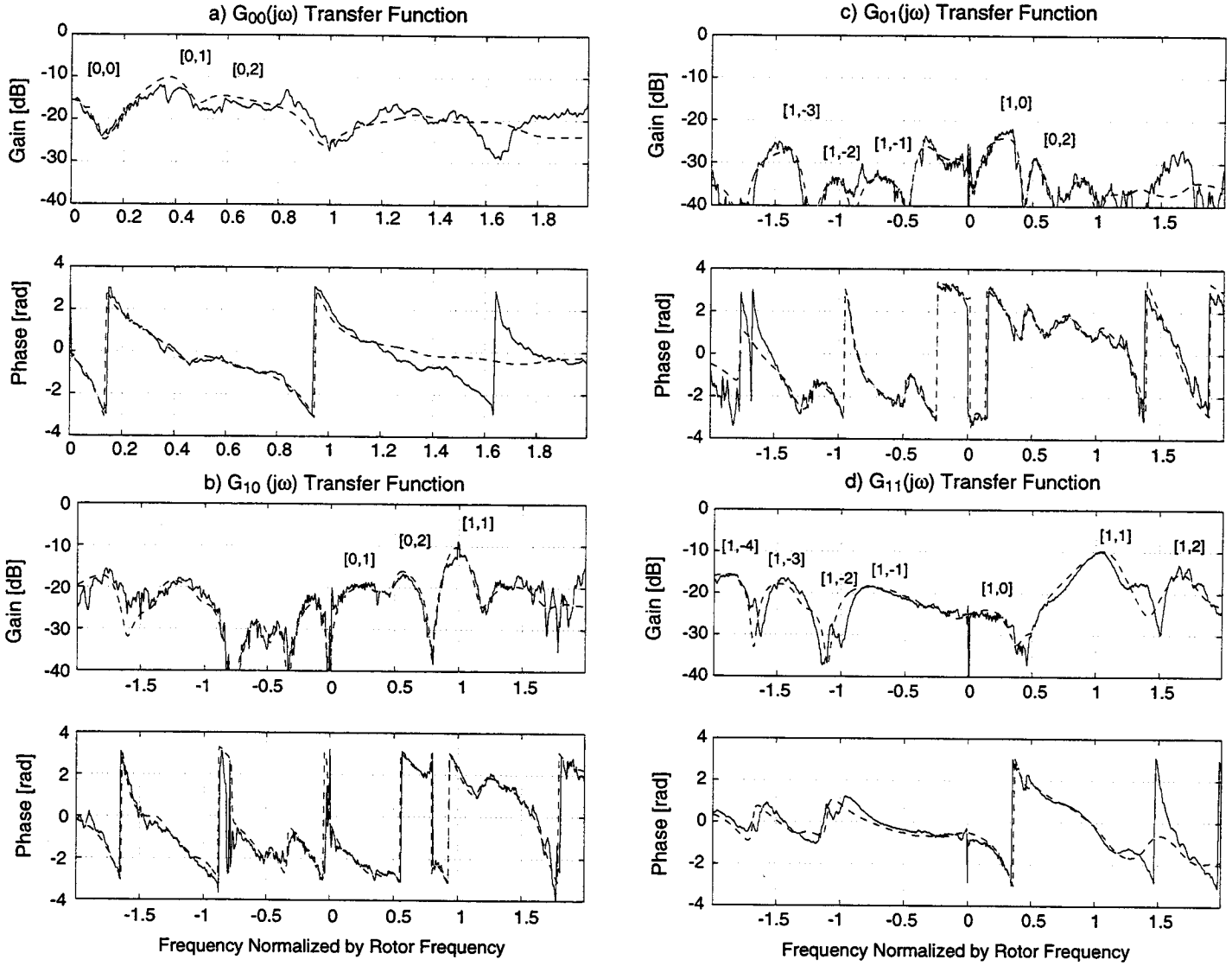

Figure 4: MIMO transfer functions $G_{00}(j\omega)$, $G_{01}(j\omega)$, $G_{10}(j\omega)$, and $G_{11}(j\omega)$, with circumferential inlet distortion at $\dot{m}_{corr}$ = 16.0 kg/s and 85% corrected design speed. —— = measured, – – = identified model.

Mode number assignment requires careful data reduction and analysis. First, to visualize the spatial structure of the modes, we reconstruct the mode shapes using the eigenstructure of the identified state-space model (Spakovszky (1998)). Figure 5 shows some of the reconstructed mode shapes, including the harmonic content in each. For these experiments the distortion screen ranged from 180° to 300° — this is marked with ×'s in Figure 5. Next, we assign the number n based on the harmonic which contributes most to the mode shape. The first two modes in Figure 5 have strong 0th harmonics, indicating that overall compression system parameters (such as duct lengths and plenum size) will have a strong influence on their stability. The second two modes have strong 1st harmonics, and we will see that stabilization of these modes can be achieved by controlling the first harmonic of the flow perturbations. Finally, the "acoustic" mode number m is assigned by looking at various factors. Higher frequencies are considered to be more acoustically coupled, and are given larger values of m. We note that the mode shapes, and therefore the harmonic contents of each mode, is a function of time. Figure 5 thus portrays the modes at several specific instants in time. Eigenvalues obtained without distortion Weigl et al. (1997) (also see Weigl

are based only upon the input-output model.

(1997)) are compared to those found here, to judge how distortion has altered their frequency, stability, and harmonic content; this also helps to assign the mode numbers. In addition, low speed modeling (Van Schalkwyk (1996)) is employed to help associate mode numbers with the peaks when strong coupling is present. The results are summarized in Figure 6, which shows the identified poles and assigned mode numbers.

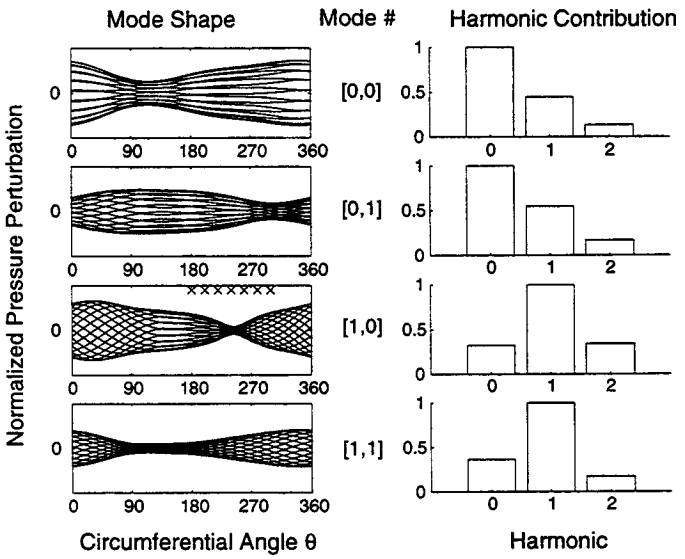

Figure 5: Left: mode shapes for the four primary modes of the identified dynamics, plotted in several positions as the eigenmode travels around the annulus. Right: amplitude of the harmonic contribution to each mode, indicating which harmonic dominates and the degree of coupling between harmonics. Vertical scales are arbitrary, since only the mode shape is shown.

Several statements can be made based on Figure 5. First, note that mode [1,0] has a minimum at approximately 250°, which is about in the middle of the distorted region. This behavior is predicted by the low-speed model and has been observed in a low-speed compressor by Van Schalkwyk et al. (1997). Furthermore, the Fourier decompositions of the mode shapes, shown in the right hand graphs of Figure 5, indicate that several harmonics are present in each mode; this is also predicted by incompressible theory. The compressible modes [0,1] and [1,1], on the other hand, represent an effect which has not yet been modeled: it appears that these higher frequency, compressible dynamics are also coupled, to an extent very similar to the incompressible dynamics, by inlet distortion. Finally, we note that the richness of the dynamics displayed in Figure 4 and Figure 5 makes the control problem more complex, but this complexity is mitigated by the fact that some of the high frequency

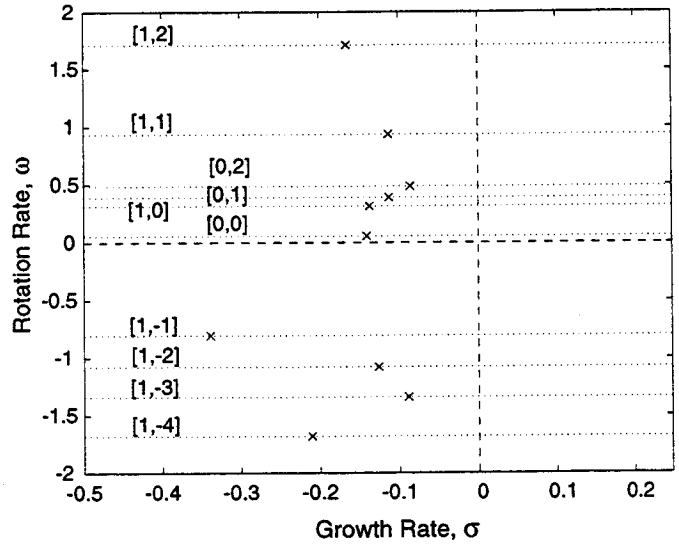

Figure 6: Identified poles of the multi-variable transfer function system at $\dot{m}_{corr} = 16.0$ kg/s.

modes are relatively well damped, and do not tend to go unstable as mass flow is reduced.

To study the relative stability and sensitivity to mass flow of the various compressor modes, we conducted system identification at various mass flows. By comparing all of the transfer functions at all the tested mass flows, it was found that the [1,0] mode is primarily responsible for system stability. To summarize our conclusion, Figure 7 shows the magnitude and phase of G_{11} measured at four different mass flows. The [1, 0] mode is particularly visible in this transfer function. Only the positive frequency (forward traveling wave) portion of the transfer functions are shown. As the mass flow is decreased, the magnitude of the peak at $0.4\omega_r$ increases, indicating a lightly damped mode. At the lowest mass flow tested this mode is actually unstable. This can be determined by looking at the corresponding phase plot: for $\dot{m}$ =14.0 kg/s (solid line), the phase increases in the range $0.3 \leq \omega_r \leq 0.6$, indicating that the pole associated with this mode is unstable. For $\dot{m}$ =15.0 kg/s (dash-dot) and 14.7 kg/s (dash) the respective phases decrease in the same frequency range, indicating that at these mass flows the mode is stable. Note that for $\dot{m}$ =16.0 kg/s (dotted) the phase also increases in this frequency range. However, at this high mass flow the mode is stable. The increase in the phase is a result of a zero at $0.35\omega_r$ which is clearly visible as a deep valley in the magnitude of the transfer function.

Note that the compressible modes in Figure 7 (labeled [1, 1] and [1, 2]) do not change significantly with mass

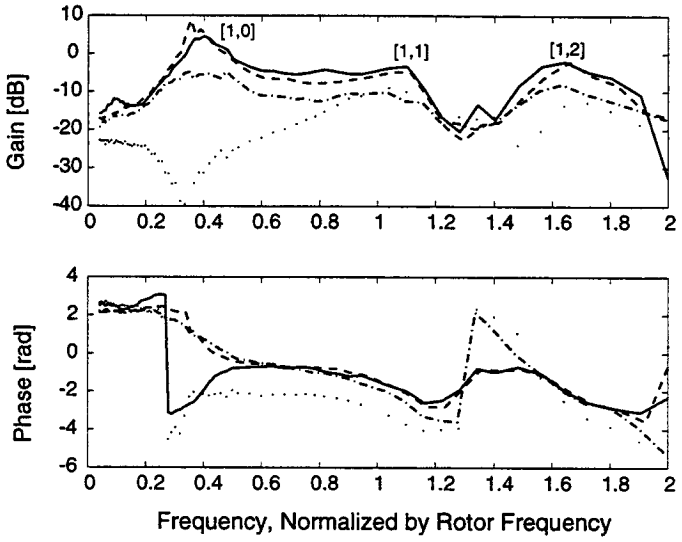

Figure 7: Measured $G_{11}(j\omega)$ at 16.0 kg/s (dotted), 15.0 kg/s (dash-dot), 14.7 kg/s (dash) and 14.0 kg/s (solid) total corrected mass flow.

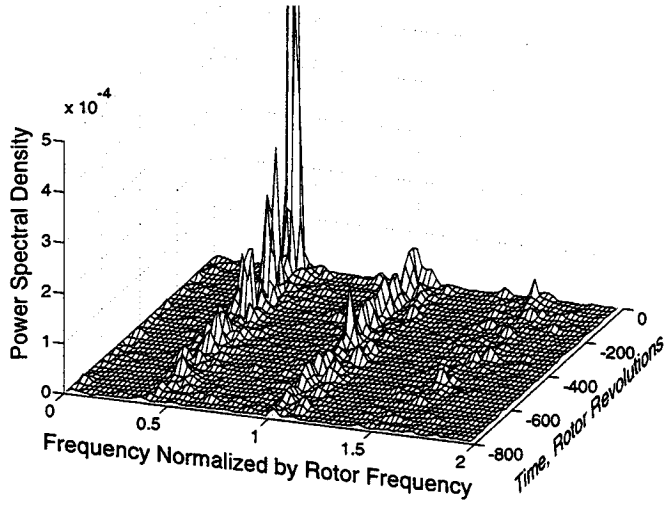

Figure 8: Spectrogram of the 1st harmonic perturbations during an open loop stall ramp.

flow. These eigenmodes cause peaks in the transfer function which change only slightly as the mass flow is decreased, indicating that their degree of stability is not greatly affected by the decrease in mass flow. Similar conclusions were drawn about other pre-stall modes by looking at the relevant transfer functions and studying eigenvalue migration with mass flow.

Throttle ramps into stall revealed that indeed the $[1,0]$ mode resonates strongly as the stall point is approached. This mode can be related to the incompressible Moore-Greitzer mode, and has also been observed with radial distortion in Part I (Spakovszky et al. (1998)). The spectrogram of the first harmonic of the pressure perturbations during a stall event is plotted in Figure 8. We note that, even right up to stall, there is relatively little activity at $1\omega_r$ and $1.6\omega_r$. This indicates the [1,1] and [1,2] compressible modes are well damped and that it is the [1,0] mode that loses stability.

In summary, in the presence of circumferential distortion, the stability of the compression system is determined by the [1,0] mode. This behavior is analogous to that observed in low-speed compressors. The additional compressible modes were also observed with radial distortion by Spakovszky et al. (1998). Unlike radial distortion, there is strong *coupling* between the harmonics, that is, each mode contains several harmonics. This coupling is considered during design and testing of controllers to stabilize the compression system, discussed in the next section.

5. Active Control Results

In this section we discuss active control of rotating stall in a high-speed single-stage compression system with circumferential distortion. Two different controllers were tested: a constant gain controller, and a dynamic, model based controller. The two controllers are discussed in the following sections.

5.1 Constant Gain Control

Constant gain control has been used successfully by several researchers to stabilize rotating stall in low-speed compressors. Paduano et al. (1993) developed the experimental design procedure on a single-stage compressor, and Haynes et al. (1994) applied it to a three-stage compressor. The same approach was used by Van Schalkwyk et al. (1997) to stabilize a three-stage compressor with circumferential distortion of the inlet total pressure. However, Weigl et al. (1997) showed that constant gain controllers are not effective in high-speed compressors with uniform inlet flow. A similar result was obtained in Part I (Spakovszky et al. (1998)) with radial distortion. However, as we will see momentarily, constant gain control was very effective on this machine in the presence of circumferential distortion.

The idea behind constant gain control is as follows. The circumferential pressure perturbation $\delta p(\theta)$ is measured and decomposed in a Fourier series analogous to Equation (3). The nth harmonic is then spatially rotated by an experimentally optimized angle β_n, multiplied by a constant gain k_n to form the nth harmonic of the control signal. For ex-

ample, for a sensed first harmonic perturbation $\widetilde{y}_1 = \delta\widetilde{p}_1$ the constant gain control law is

$$\widetilde{u}_1 = -k_1 e^{j\beta_1}\delta\widetilde{p}_1 \tag{10}$$

where $\widetilde{u}_1$ is the corresponding first harmonic SFC of the injection wave. Finally, the individual actuator commands are reconstructed based on the Fourier coefficients.

A first harmonic constant gain control law was found to be effective at stabilizing the circumferential distortion case investigated here. When the gain and phase were set to $k_1 = 1$ and $\beta_1 = \pi$ respectively, the stalling mass flow was reduced by 6.8% relative to steady blowing. The total-to-static speed lines are plotted in Figure 9 for undistorted inlet flow (solid), circumferential distortion without blowing (dash), and with 50% steady blowing (dash-dot). The stall

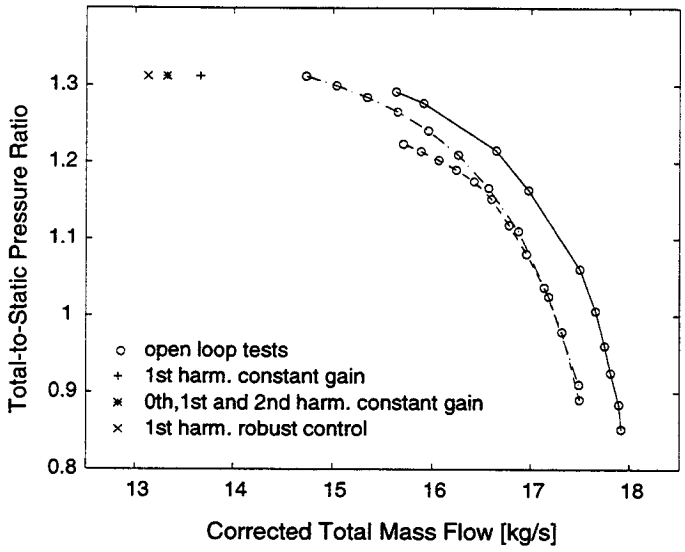

Figure 9: Speed lines for undistorted inlet flow (solid), circumferential distortion without blowing (dash), and with 50% steady blowing (dash-dot). Stall points with control are: 1st harmonic constant gain control (+), 0th-1st-2nd harmonic constant gain control (∗), and 1st harmonic H_∞ control (×).

point with the first harmonic constant gain control law is marked with a + in this figure.

Spectrograms of the first and second harmonics of the pressure perturbations, immediately prior to the control-on stall point, are shown in Figures 10 and 11 respectively. The $[1,0]$ mode appears to be relatively well damped during the first 1000 revolutions in Figure 10, while the $[1,1]$ mode and the $[2,0]$ mode (Figure 11) are resonating strongly during the entire pre-stall period. Other evidence indicates that the $[2,0]$ mode goes unstable first, and in fact adding

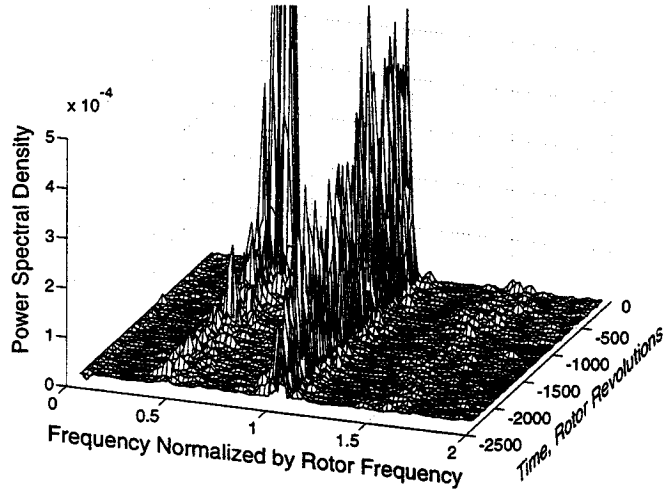

Figure 10: Spectrogram of the first harmonic pressure perturbations with first harmonic constant gain control.

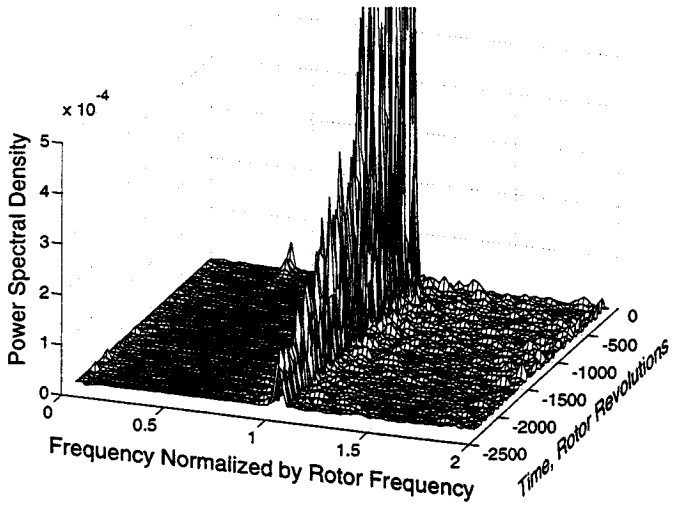

Figure 11: Spectrogram of the second harmonic pressure perturbations with first harmonic constant gain control.

a second harmonic constant gain feedback with $k_2 = 1$ and $\beta_2 = \pi$ damped out the second harmonic mode and achieved a further range extension of 2.2% in stalling mass flow relative to the first harmonic constant gain control case. The measured mass flow and pressure ratio is marked with a $*$ in Figure 9. A zeroth harmonic feedback, with gain $k_0 = 1$, is also in operation during this run.

These results clearly show that constant gain control is effective in the presence of circumferential distortion. Since a compressible, distorted flow, control theoretic model

does not exist, it is difficult to explain these phenomena. The system identification experiments indicate that a single mode with dominant first harmonic and incompressible features determines the stability, suggesting the applicability of a constant gain control strategy. This was also qualitatively and quantitatively verified using incompressible modeling methods (Van Schalkwyk (1996)). However, the measurements in Figure 4 show that there are *compressible* modes that have significant magnitudes in the coupled (off-diagonal) transfer functions (e.g. the [1, 1] mode has the same magnitude in $G_{11}(j\omega)$ as in $G_{10}(j\omega)$). Such coupling is typically detrimental to any control law which does not explicitly take it into account. Even without this coupling, the [1, 1] mode in this compressor has invariably been destabilized by constant gain control without circumferential distortion (Weigl et al. (1997), Spakovszky et al. (1998)). Apparently the effect of distortion in this machine is such that the constant gain control law, tuned for mode [1, 0] stabilization, does not destabilize the other lightly damped modes. It is not clear whether this fortuitous effect will exist in other compressors with inlet distortion.

5.2 Robust H_∞ Control

In this section the performance improvement obtained using robust H_∞ control is investigated. As in Part I (Spakovszky et al. (1998)), the lack of a theoretical model requires the use of an identified model for the design of these model-based dynamic control laws. This is particularly difficult when circumferential distortion is present, because the compressor becomes a MIMO dynamic system in which one common set of eigenmodes describes the coupled compressor dynamics; in other words, one cannot treat one harmonic at a time. This complicates system identification and significantly increases the order of the controller. Because of this added complexity, initial tests of a MIMO H_∞ controller did not show an improvement in stalling mass flow over constant gain control (Spakovszky (1998)). Although further iteration and improvement of the MIMO controller design should be possible, time did not permit this approach to be pursued. Therefore an alternative method, described below, was investigated.

The dominance of the first harmonic in the [1,0] mode and the presence of a resonance in the [1,1] mode in Figure 10 suggests that a robust controller which ignores coupling, and is designed for the first harmonic only, might yield improvement in performance. Fortunately, such a controller already existed at the time of these tests, because the frequencies associated with the [1,0] mode for both circumferential and radial distortion are approximately the same ($0.4\omega_r$). In fact, the eigenvalue location of the unstable [1,0] mode used for design of the radial distortion controller was almost identical to the identified eigenvalue location for this mode with distortion. Figure 12 shows the identified eigenvalues with circumferential distortion, together with circles indicating the range of eigenvalues which the first harmonic H_∞ radial distortion controller from Part I (Spakovszky et al. (1998)) was designed to stabilize. The

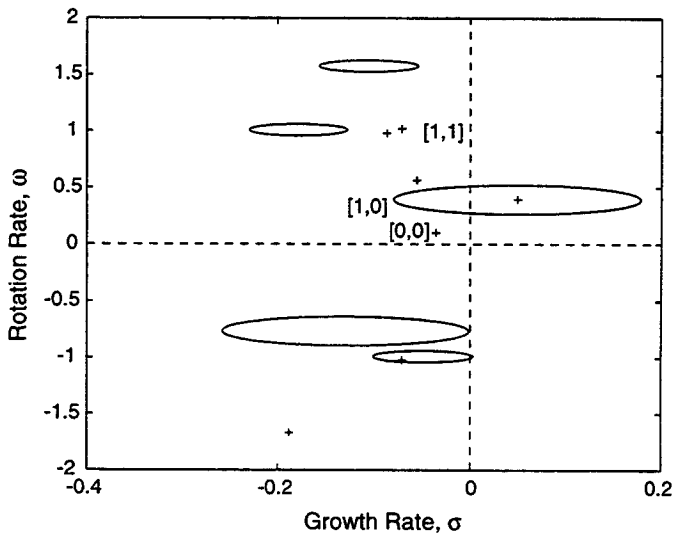

Figure 12: Identified coupled unstable dynamics at $\dot{m}_{corr}$ = 14.0 kg/s and perturbation circles of H_∞ control law designed for radial distortion.

[1,0] mode perturbation circle includes the unstable pole associated with circumferential distortion, indicating that the controller should be able to stabilize this mode. Although the [1, 1] mode with circumferential distortion is more lightly damped than in the design model, the frequency is accurately captured by the design model. This proves to be sufficient for success of the controller, indicating that this pole remains stable for the mass flows of interest.

Based on these arguments the controller originally designed for radial distortion was tested experimentally and showed a large range extension. The stalling mass flow was reduced by 10.2% relative to steady blowing, resulting in a total reduction in stalling mass flow of 16.4%. This is indicated in Figure 9. Of all the methods tested, this first harmonic robust control law achieved the largest reduction in stalling mass flow, which is comparable to the reduction in stalling mass flow with radial inlet distortion shown in Part I (Spakovszky et al. (1998)).

6. Concluding Remarks and Summary

This paper presents the first experimental investigation of coupled compressible stall dynamics and it is the first time that a transonic compressor with circumferential inlet distortion was actively stabilized. The distortion magnitude was about one dynamic head, corresponding to DC(60)=0.61.

Forced response experiments revealed strong coupling between the harmonics of the pressure perturbations. Analysis showed that a single mode of the compression system determines its stability — this behavior is similar to that of low-speed compressors. Constant gain control achieved a large range extension. The dominance of an incompressible mode, together with fortuitous coupling between the harmonics, appears to change the stall dynamics in such a way that (unlike the undistorted flow case) constant gain feedback does not destabilize lightly damped compressible modes. Thus, although the details of the measured dynamics are strongly affected by compressibility, the control strategy applied here was the same as that used in low-speed compressors. The maximum reduction in stalling mass flow with zeroth, first and second harmonic constant gain controllers was 9.0% relative to steady blowing, giving a total reduction in stalling mass flow of 15.2%.

In general, a MIMO control law is indicated when coupled multi-variable dynamics are present. In this experiment, however, the dominance of the first harmonic in the destabilizing mode suggested that a SISO H_∞ controller for the first harmonic might work well. This in fact proved to be the case: a controller originally designed for radial distortion achieved a total reduction in stalling mass flow of 16.4%, thus demonstrating robustness with respect to a change in inlet flow from radial to circumferential distortion. Time did not permit comparing this performance to a MIMO controller.

These results, together with the results of Part I (Spakovszky et al. (1998)), show that active control of rotating stall in a high-speed compressor results in a significant increase in the stable operating range of a compressor operating in the presence of inlet distortion. These results are very promising for future work and applications. Much work remains to be done, however. In particular, the dependence of the dynamics on nonlinear coupling between the compressor and a (typically unknown) inlet distortion add a degree of uncertainty which is addressed in our approach only to the extent that our control law is robust to modeling errors. More explicitly designing for, and subsequently testing against, unknown distortion scenarios are needed. It is also necessary to investigate and better understand the interplay between distortion and lightly damped compressible dynamics. This interplay was beneficial in these experiments, but may not always be so. Finally, one would like to use as few actuators and as little mass flow as possible to achieve results like those presented here, and do so in a multistage high-speed environment.

7. Acknowledgments

This project was conducted under collaboration between the NASA Lewis Research Center, Scientific Systems Co., Inc., and MIT. The authors would like to thank T. Strazisar and J. Chi for their very useful input, as well as D. Williams, R. Brokopp, and B. Piendl for their help during compressor testing. Special thanks also to M. Carroll and D. Park for preparing this manuscript. This work was conducted under NASA funding NAG3-1457 and NAS3-97100.

References

Berndt R., Weigl H., Paduano J., and Epstein A., 1995. "Experimental Techniques for Actuation, Sensing, and Measurement of Rotating Stall Dynamics in High Speed Engines." In J.D. Paduano (editor), *Sensing, Actuation, and Control in Aeropropulsion*, vol. 2492. SPIE.

Bonnaure L., 1991. *Modelling High Speed Multistage Compressor Stability.* Master's thesis, Department of Aeronautics and Astronautics, MIT.

Feulner M., Hendricks G., and Paduano J., 1994. "Modeling for Control of Rotating Stall in High Speed Multi-Stage Axial Compressors." In *ASME Gas Turbine and Aeroengine Congress and Exposition, The Hague, The Netherlands, Paper 94-GT-292.*

Haynes J., Hendricks G., and Epstein A., 1994. "Active Stabilization of Rotating Stall in a Three-Stage Axial Compressor." *ASME J. of Turbomachinary*, vol. 116 pp. 226–239.

Hendricks G., Bonnaure L., Longley J., Greitzer E., and Epstein A., 1993. "Analysis of Rotating Stall Onset in High Speed Axial Flow Compressors." In *AIAA/SAE/ASME/ASEE 29th Joint Propulsion Conference, Paper AIAA-93-2233.*

Hynes T. and Greitzer E., 1987. "A method for assessing Effects of Circumferential Flow Distortion on Compressor Stability." *ASME J. of Turbomachinary*, vol. 109 pp. 371–379.

Jacques R., 1994. *On-line System Identification and Control Design for Flexible Structures.* Ph.D. thesis, Department of Aeronautics and Astronautics, MIT.

Koch C.C., 1970. "Experimental Evaluation of Outer Case Blowing or Bleeding of a Single-Stage Axial Flow Compressor." Tech. Rep. CR-54592, NASA.

Ljung L., 1987. *System Identification: Theory for the User.* Prentice-Hall, Inc.

Longley J. and Greitzer E., 1992. "Inlet Distortion Effects in Aircraft Propulsion System Integration." *Steady and Transient Performance Prediction of Gas Turbine Engines, AGARD-LS-183* pp. 6-1 – 6-18.

Moore F. and Greitzer E., 1986. "A Theory of Post-Stall Transients in Axial Compressors: Part I — Development of the Equations." *ASME J. of Engineering for Gas Turbines and Power*, vol. 108 pp. 68–76.

Paduano J., Epstein A., Valavani L., Longley J., Greitzer E., and Guenette G., 1993. "Active Control of Rotating Stall in a Low-Speed Axial Compressors." *ASME J. of Turbomachinary*, vol. 115 pp. 48–56.

Reid L. and Moore D., 1978. "Performance of Single-Stage Axial-Flow Transonic Compressor With Rotor and Stator Aspect Ratios of 1.19 and 1.26, Respectively, and With Design Pressure Ratio 1.82." Tech. Rep. TP-1338, NASA.

Spakovszky Z., 1998. "Active Control of Rotating Stall in NASA Compressor Stage 35 with Inlet Distortion." Master's thesis in preparation, Department of Aeronautics and Astronautics, MIT.

Spakovszky Z., Weigl H., Paduano J., Van Schalkwyk C., Suder K., and Bright M., 1998. "Rotating Stall Control in a High-Speed Stage with Inlet Distortion, Part I — Radial Distortion." In *ASME Gas Turbine and Aeroengine Congress and Exposition, Stockholm, Sweden.*

Van Schalkwyk C., 1996. *Active Control of Rotating Stall with Inlet Distortion.* Ph.D. thesis, Department of Aeronautics and Astronautics, MIT. Also available as Gas Turbine Lab Report #222.

Van Schalkwyk C., Paduano J., Greitzer E., and Epstein A., 1997. "Active Stabilization of Axial Compressors with Circumferential Inlet Distortion." In *ASME Gas Turbine and Aeroengine Congress and Exposition, Orlando, FL, Paper 97-GT-279.*

Weigl H., Paduano J., Fréchette L., Epstein A., and Greitzer E., 1997. "Active Stabilization of Rotating Stall and Surge in a Transonic Single Stage Axial Compressor." In *ASME Gas Turbine and Aeroengine Congress and Exposition, Orlando, FL, Paper 97-GT-411.*

Weigl H.J., 1997. *Active Stabilization of Rotating Stall and Surge in a Transonic Single Stage Axial Compressor.* Ph.D. thesis, Department of Aeronautics and Astronautics, MIT.

Williams D., 1991. "Engine Compatibility." Tech. rep., Rolls-Royce PLC.